AIP Journal of Applied Physics

Phase evolution and room-temperature photoluminescence in amorphous SiC alloy

H. P. Zhou, M. Xu, D. Y. Wei, T. Ong, S. Q. Xiao et al.

Citation: J. Appl. Phys. **111**, 103526 (2012); doi: 10.1063/1.4721412
View online: http://dx.doi.org/10.1063/1.4721412
View Table of Contents: http://jap.aip.org/resource/1/JAPIAU/v111/i10
Published by the AIP Publishing LLC.

Additional information on J. Appl. Phys.

Journal Homepage: http://jap.aip.org/
Journal Information: http://jap.aip.org/about/about_the_journal
Top downloads: http://jap.aip.org/features/most_downloaded
Information for Authors: http://jap.aip.org/authors

ADVERTISEMENT

Downloaded 17 Jul 2013 to 155.69.4.4. This article is copyrighted as indicated in the abstract. Reuse of AIP content is subject to the terms at: http://jap.aip.org/about/rights_and_permissions

Phase evolution and room-temperature photoluminescence in amorphous SiC alloy

H. P. Zhou,[1] M. Xu,[2] D. Y. Wei,[1] T. Ong,[1] S. Q. Xiao,[1] L. X. Xu,[1] S. Y. Huang,[1] Y. N. Guo,[1] S. Khan,[1] and S. Xu[1,a)]
[1]*Plasma Sources and Application Center, NIE, Nanyang Technological University, Singapore 637616 and Institute of Advanced Studies, Nanyang Technological University, Singapore 637616*
[2]*Key Lab of Information Materials of Sichuan Province & School of Electrical and Information Engineering, South-West University for Nationalities, Chengdu 610041, China*

(Received 21 February 2012; accepted 23 April 2012; published online 25 May 2012)

Amorphous SiC thin films with varying phases and compositions have been synthesized using a low frequency inductively coupled high density plasma source in a hydrogen diluted methane (CH_4) and silane (SiH_4) mixture. The optical and electrical properties along with the microstructures of the thin films are systematically investigated. The feedstock gas ratio of CH_4/SiH_4 leads to the fluctuations of the optical bandgap, the carbon content, and the transition of Si–Si bonding structure from crystalline to intermediate phase and finally to amorphous phase. Room temperature photoluminescence (PL) with nearly fixed emission energy has been observed in the thin films. The underlying PL mechanism is explained in the framework of quantum confinement-luminescence center model. The photoexcitation process occurs in the nc-Si quantum dots embedded in the host SiC matrix, whereas the photoemission process occurs in the luminescence centers in the surrounding SiC or at SiC-Si interfaces. The PL evolution with the chemical composition in the films is analyzed in terms of the density of the Si quantum dots and the Si–C bond. © *2012 American Institute of Physics*. [http://dx.doi.org/10.1063/1.4721412]

I. INTRODUCTION

Amorphous silicon carbide (a-Si_xC_{1-x}) has attracted increasing interests in a wide range of applications in microelectronic and photonic devices, e.g., photodetector, and light-emitting diodes (LEDs).[1] The distinguished property which makes silicon carbide so attractive is the tunability of its optical band gap, which can be altered from 1.9 to 3.6 eV by simply controlling the carbon content. In photovoltaic devices, this material has already been employed to serve as the window layer of n-i-p thin film solar cells,[1] giving an energy conversion efficiency (η) of about 8%. It has also been used as emitter of the Si-base heterojunction solar cells yielding an energy conversion efficiency of 15%.[2] Recently, SiC has been successfully applied for silicon surface passivation to suppress the surface recombination velocity to the level as low as 30 cm/s.[3]

Incorporation of carbon into a-Si:H thin films improves the optical properties in n-i-p thin film or heterojunction solar cells because of the widening of the optical band gap. However, formation of silicon-carbon bonds often deteriorates the electronic properties of the thin films due to the occurrence of C-related defects.[4] Therefore, there is a compromise between the optical and electronic properties of the a-Si_xC_{1-x}:H thin films. There has not been a systematic understanding of the nature of electronic passivation of a-Si_xC_{1-x}:H on monocrystalline silicon yet. However, it is recognized that the passivation effect is strongly dependent on the deposition parameters, the carbon/hydrogen content, the inner bonding configuration, etc.[3] For example, Ehling *et al*. observed that the minority carrier effective lifetime of the Si surface passivated with a-SiC:H thin films is temperature sensitive due to the difference of the microstructure of a-SiC:H layers.[5] Indeed, the phase and bond evolution with chemical composition in a-SiC:H is significant for the improvement of the energy conversion efficiency of solar cells.

Silicon quantum dots (QDs) or nanograin silicon embedded in a dielectric host matrix (Si_3N_4, SiO_2, and SiC) is another attractive venue for the composite of a-Si_xC_{1-x}:H. In comparison with Si QDs embedded in Si_3N_4 or SiO_2 matrices, the Si QDs embedded in the SiC matrix are trapped in the potential barrier with height of ~2.5 eV, significantly lower than that of Si_3N_4 (~5.3 eV) and SiO_2 (~9 eV). It implies that this system is favorable for the carrier transport and effective luminescence of Si QDs. This is because the tunneling probability of the carriers between the adjacent Si QDs in the SiC matrix can be exponentially increased, and the radiative electron-hole recombination rate can be significantly enhanced due to the strong overlap of electron-hole wave functions.[6,7] In our previous works, Si QDs in an amorphous SiC matrix were investigated.[8] The formation mechanism of Si QDs is explained as the hydrogen dilution effect on the nucleation and growth processes of the Si QDs in the used ultra-high density low frequency inductively coupled plasma (LFICP) source.

In this work, the a-SiC thin films were fabricated by using LFICP (460 kHz) source with feedstock gases of H_2 diluted SiH_4 and CH_4. The flow rate of SiH_4 and hydrogen was kept constant and that of CH_4 was varied. The silicon phase transition and inner bonding structure evolution with increasing gas ratio of CH_4/SiH_4 were systematically

a)Author to whom correspondence should be addressed. Electronic mail: shuyan.xu@nie.edu.sg.

0021-8979/2012/111(10)/103526/7/$30.00

© 2012 American Institute of Physics

Downloaded 17 Jul 2013 to 155.69.4.4. This article is copyrighted as indicated in the abstract. Reuse of AIP content is subject to the terms at: http://jap.aip.org/about/rights_and_permissions

investigated. Moreover, the infrared photoluminescence from the thin films was observed and explained using the quantum confinement-luminescence center (QCLC)[9] model based on a variety of bond structure characterization techniques including x-ray photoelectron spectroscopy (XPS), Raman scattering, and others.

II. EXPERIMENTAL DETAILS

The a-SiC thin films were deposited on glass and double-side polished silicon substrates (resistivity of 12 Ω cm) in the LFICP system.[8] In order to further minimize the surface defect from the ion bombardment, the distance between the flat coil antenna and the substrate stage was increased from 11 cm to 31 cm by extending the height of the reactive chamber. A routine base pressure of $\sim 2 \times 10^{-4}$ Pa was maintained in the reaction chamber by a combination of a rotary and a turbo-molecular pump. The flow rates of silane and hydrogen were kept constants at 5 and 20 sccm (sccm denotes cubic centimeter per minute at standard temperature and pressure), respectively. The flow rate of methane was varied from 0 to 5 sccm, corresponding to the flow rate ratio ($R = CH_4/SiH_4$) of 0, 0.2, 0.4, 0.6, 0.8, and 1, respectively. The substrates were placed on a carrier stage mounted with a thermal couple. Throughout the deposition process, the substrate temperature was kept at 400 °C. The inductive RF discharge power density, the total working pressure in the chamber, and the deposition duration were maintained at 21 mw/cm^3, 7.8 Pa, and 60 min, respectively.

The thickness of the thin films was measured directly from the cross-sectional scanning electron microscopy (SEM) image. The deposition rate can be calculated from the thickness divided by deposition duration. The microstructures of the thin films were characterized by x-ray diffraction (XRD) (Siemens D5005, incidence line of Cu Kα with wavelength of 1.54 Å) and Raman scattering (Renishaw 1000 micro-Raman with a 514.5 nm Ar^+ laser for excitation). Room temperature photoluminescence was recorded by the same Raman system with incident power of 25.8 mW. Fourier transform infrared (FTIR) and UV-VIS–near IR transmission spectra were employed to study the Si–H bond configuration and optical band gap of the samples, respectively. FTIR measurement was performed on a Perkin-Elmer FTIR 1725X spectrometer in the mid-infrared range from 400 to 3200 cm^{-1} with increment of 1 cm^{-1}. The Cary 510 Bio spectrometer (300–1100 nm) was used to measure the UV-VIS–near IR transmission spectra. The chemical composition and bonding states of the deposited thin films were studied *ex situ* by VG ESCALAB 220I-xl x-ray photoelectron spectrometer using a Mg Kα (1253.6 eV) x-ray source. The conductivity of the thin films was measured using a Keithley 4200 SCS system in combination with a Keithley 2635 A system sourcemeter.

III. EXPERIMENTAL RESULTS

A. Surface morphology of the a-SiC thin films

The top-view SEM images of the deposited a-SiC thin films are shown in Fig. 1. The samples in Figs. 1(a)–1(f) were deposited at constant flow rates of SiH_4 (5 sccm) and H_2 (20 sccm) and varying gas ratio R from 0 to 1 with an increment of 0.2. From these images, one can see that the surfaces of the thin films are similar and uniformly covered by compact small particles without any observable voids between

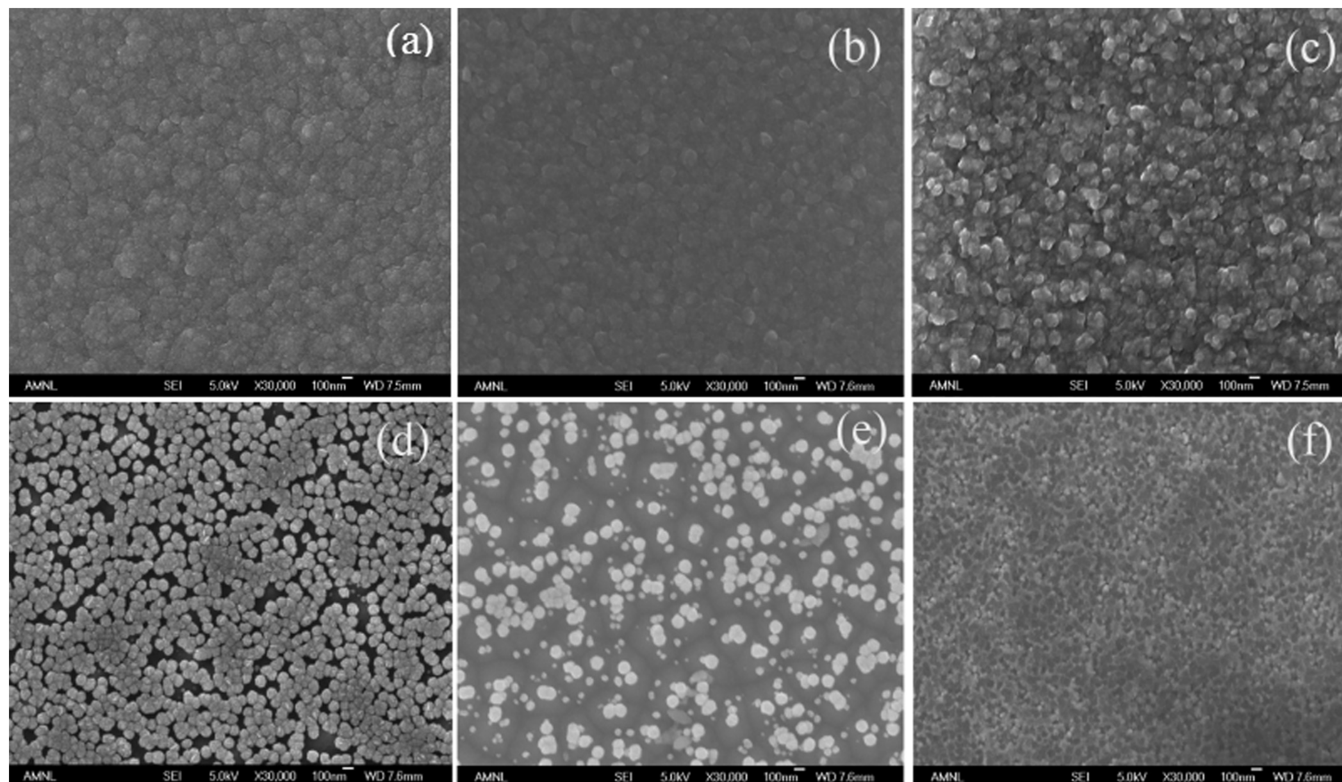

FIG. 1. The surface morphologies of the thin films deposited at different gas ratios of CH_4/SiH_4.

Downloaded 17 Jul 2013 to 155.69.4.4. This article is copyrighted as indicated in the abstract. Reuse of AIP content is subject to the terms at: http://jap.aip.org/about/rights_and_permissions

them when R is in the range of 0–0.4 [$R = 0$ in Fig. 1(a), 0.2 in Fig. 1(b), and 0.4 in Fig. 1(c)]. The corresponding cross-sectional images exhibit a columnar structure, which is usually observed in amorphous or microcrystalline silicon growth.[10] This indicates a possible preferential growth direction perpendicular to the substrate. The vertical alignment of the columnar structure is beneficial to the effective carrier transport through providing transport channel.[11] Interestingly, when the ratio is increased to 0.6 [Fig. 1(d)], spherical shaped grains with tens of nanometers size appear on the surface. In addition, some voids appear between these small grains. Further increasing the ratio CH_4/SiH_4 to 0.8 [Fig. 1(e)] causes the distance between the grains to increase. Finally, when the flow rate of methane is set to equal to that of silane [Fig. 1(f)], the grid network structures are formed. It appears to be the result of separation of two different phases.

B. UV-VIS-near IR transmission spectra

In order to obtain information of the optical properties of the deposited thin films, the UV-VIS-near IR transmission measurement was performed in the spectra range of 300-1000 nm as displayed in Fig. 2(a). In the case of low gas ratios R, evident light interference fringes due to multi-layer structures are observed. The optical band gap E_g for indirect semiconductor can be deduced from the Tauc equation[12] $(\alpha h\nu)^{1/2} = B(h\nu - E_g)$, where α is the absorption coefficient, $h\nu$ the photon energy, and B is a constant related to the width of the band tails or disorder in the film in terms of band length distribution and angle. The obtained values of the optical band gap E_g, together with the deposition rate versus flow rate ratio, are plotted in Fig. 2(b). The E_g value of silicon thin film is 1.68 eV (in the absence of methane), which is larger than that of the Si thin film (~1.3 eV) previously deposited under similar conditions except the distance between the antenna and the substrate.[13] The optical band gap of hydrogenated amorphous silicon depends on the crystallinity and hydrogen content.[14] Considering the low hydrogen content in present thin films (see FTIR results), the wider optical band gap is attributed to the comparatively lower crystallinity because of the increase of the distance between the antenna and the substrate. With the incorporation of methane up to $CH_4/SiH_4 = 0.6$, E_g monotonously rises from 1.68 to 2.26 eV and the deposition rate decreases from 23.8 to the minimum value of 1.7 nm/min. One can notice that E_g encounters a slight shrinkage, while R starts to rise in the gas ratio range of 0.6–0.8. The change of optical band gap and deposition rate with the gas ratio of CH_4/SiH_4 is connected with the phase evolution in the thin films, which will be further discussed in the subsequent sections.

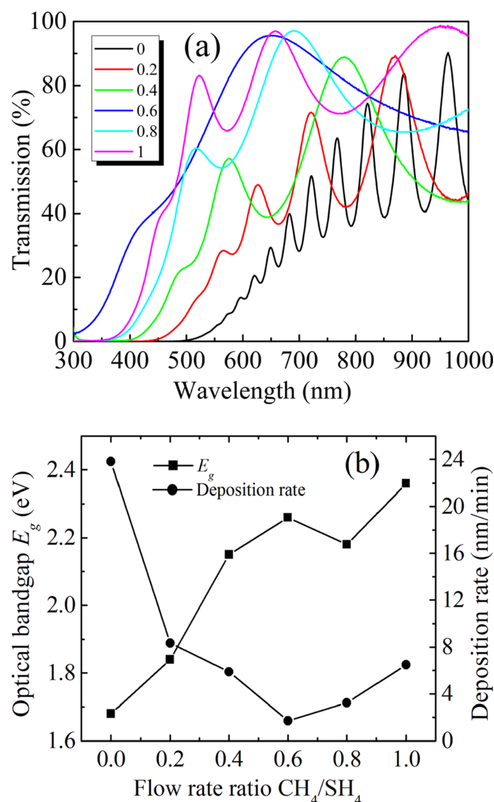

FIG. 2. The UV-VIS transmission spectra of the thin films deposited at different gas ratios of CH_4/SiH_4.

C. X-ray diffraction

The XRD measurement was conducted to study the crystalline structure of the thin films. The diffraction patterns are represented in Fig. 3. Three pronounced diffraction peaks located at $2\theta = 28.4°$, $47.4°$, and $55.8°$ are observed at lower ratios of $CH_4/SH_4 = 0$, 0.2, and 0.4, respectively. These peaks are conclusively attributed to (111), (220), and (311) crystallographic orientation of silicon, respectively. The full width at half maximum of the peaks becomes larger with increasing methane composition in the feedstock gas, which implies the average size shrinkage of the silicon grains (from ~26 to ~18 nm estimated from the known Scherrer's formula). When the gas ratio is increased to $CH_4/SH_4 = 0.6$ and above, these Si related diffraction peaks disappear. There are two possibilities that should be responsible for this absence: the complete amorphisation of silicon or occurrence of the small crystals particles (<3 nm) which cannot be detected by XRD method because of the broadening of the spectrum.[15] This observation will be clarified in combination with the Raman scattering results to be presented in the following demonstration. Even at the higher methane composition, no signal from

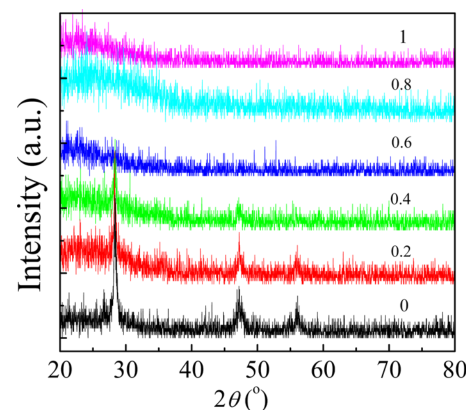

FIG. 3. The XRD patterns of the thin films deposited at different gas ratios of CH_4/SiH_4. No diffraction peaks corresponding to crystal SiC appear, indicating the amorphous nature of SiC. With the increasing content of CH_4 in the feedstock gases, Si changes from crystal to amorphous structure.

Downloaded 17 Jul 2013 to 155.69.4.4. This article is copyrighted as indicated in the abstract. Reuse of AIP content is subject to the terms at: http://jap.aip.org/about/rights_and_permissions

crystalline SiC appears, indicating the amorphous nature of the SiC phase in the thin films. This is consistent with our propositions on the conditions for silicon carbide crystallization: (1) high substrate temperature (>500 °C) and high power density to generate energetic particles diffusing on the surface, (2) high dilution ratio of feedstock gases SiH_4 and CH_4 with hydrogen to etch away the weak or strained surface bonds (such as sp^2 C and stressed sp^3 C or Si bonds), and (3) appropriate gas flow rate CH_4/SH_4 to ensure enough amounts of hydrogen and C radicals to balance the large difference of dissociation efficiency between SiH_4 and CH_4 molecules.[16] In the present experiment, the temperature, hydrogen dilution ratio, and the gas ratio CH_4/SH_4 are comparatively low. As a result, the amorphous structure of the silicon carbide is expected.

D. Room temperature photoluminescence

Fig. 4 shows the room temperature PL spectra of the thin films in the wavelength range of 550–1100 nm. A peak emission located at about 880 nm (1.4 eV) is observed in all the samples deposited at different gas ratios from 0 to 1. For the case of $R=0$ (pure silane), the peak is very weak. When R is raised from 0 to 0.4, the intensity of the peak steadily increases. However, when the ratio of CH_4/SH_4 is increased to 0.6, the intensity of this peak is drastically enhanced, resulting in a maximum intensity and a minimum width. The maximum of PL intensity is followed by a decrease at ratio of 0.8. When the flow rate of methane equals that of silane ($CH_4/SH_4=1$), the broad shoulder centered at around 720 nm becomes pronounced.

Although many experimental data have been reported, a clear understanding of the PL mechanism in Si-based materials is yet to emerge.[15] However, it is well established that the emission energy is dependent on the nanocrystal size[17] and that nonradiative surface defects compete with radiative process.[18] The former and latter correspond to the known pure quantum size effect (QSE)[19] and surface state models,[20] respectively. It is well-known that two crucial processes are involved in the PL occurrence: the formation of photoexcited carriers (photoexcitation process), i.e., pairs of electron and hole, and the radiative recombination of the photoexcited carriers through PL center (photoemission process). For the pure QSE model, it is claimed that both photoexcitation and the photoemission occur in the Si quantum dots. On the contrary, for the surface state model, it is believed that the photoexcitation originates from the Si quantum dot and the photoemission occurs in a special surface state. As to the surface state model, various surface species related to hydrogen and oxygen have been proposed.[15] In the present experiments, the hydrogen content in the deposited films is in a comparatively lower level evidenced by following FTIR spectra and previous quantitative calculation results.[21] Thus, the models focusing on the radicals of hydrides can be excluded. In terms of QSE model, the emission energy is expected to blueshift to high energy orientation because of the quantum confinement effect with the size shrink of the nano-particle. This is usually regarded as a verification of the dominant pole of QSE model in PL process. For example, Brongersma *et al.*[22] found the PL peak originally located at 880 nm blueshifts by more than 200 nm when the average size of the Si nano-particle reduces due to oxidation at high temperature of 1100 °C in the system of Si nano-particle embedded in SiO_2 matrix through Si^+ implantation. Here, although the average size of the crystal silicon particle reduces due to the incorporation of CH_4 into the feedstock gases, the emission energy was pinned around 880 nm with the enhancement of the emission intensity. As such, the QSE model should be ruled out in our experiments.

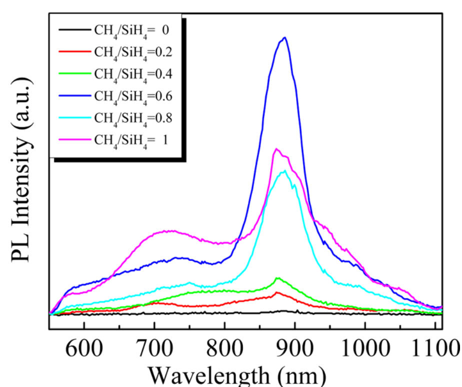

FIG. 4. Room temperature PL spectra of the thin film deposited at different gas ratios of CH_4/SiH_4. The emission peak is fixed at wavelength of about 880 nm and the maximum of PL intensity is obtained at the ratio of $CH_4/SiH_4=0.6$.

In order to get a deep understanding of the PL mechanism, the inner bonding structures of the thin films are examined by a combination of Raman scattering, FTIR, and XPS methods.

E. Raman scattering

Fig. 5(a) represents a typical Raman scattering spectrum in wide frequency shift range of 300–3000 cm^{-1}. A considerable photoluminescence background is observed for all samples except for the case of pure silane, which is consistent with the PL results in Fig. 4. The strong peaks located at 520 cm^{-1} and 970 cm^{-1} are assigned to the first- and second-order transverse optical (TO) photon vibrational modes of silicon, respectively. Simultaneously, two weak signals located at ∼1350 and ∼1580 cm^{-1} corresponding to amorphous carbon are discriminated. The former corresponds to D-band (D for disorder) and the latter the G-band (G for graphite).[23] The basic building blocks of all carbon allotropes are sp, sp^2, and sp^3 hybrid orbital. In diamond, carbon atoms form strong hybrid sp^3 orbitals. Each carbon atom is tetrahedrally coordinated with bonding angles of 109° 28′. In the graphite structure, the carbon bonds are composed of σ (sp^2 hybrid) and π (p_z). That is to say, from the Raman spectra, amorphous carbon atoms bond with each other with graphite-like configuration. Another peak centered at 2100 cm^{-1} is attributed to the SiH_2 stretching mode. In view of the whole spectra, there is not any observed Si–C bond signal due to its high bond polarizability.[24]

To investigate the bond structure of Si–Si in the composite system, a narrow range (400–600 cm^{-1}) normalized Raman spectra of the thin films deposited at different gas

Downloaded 17 Jul 2013 to 155.69.4.4. This article is copyrighted as indicated in the abstract. Reuse of AIP content is subject to the terms at: http://jap.aip.org/about/rights_and_permissions

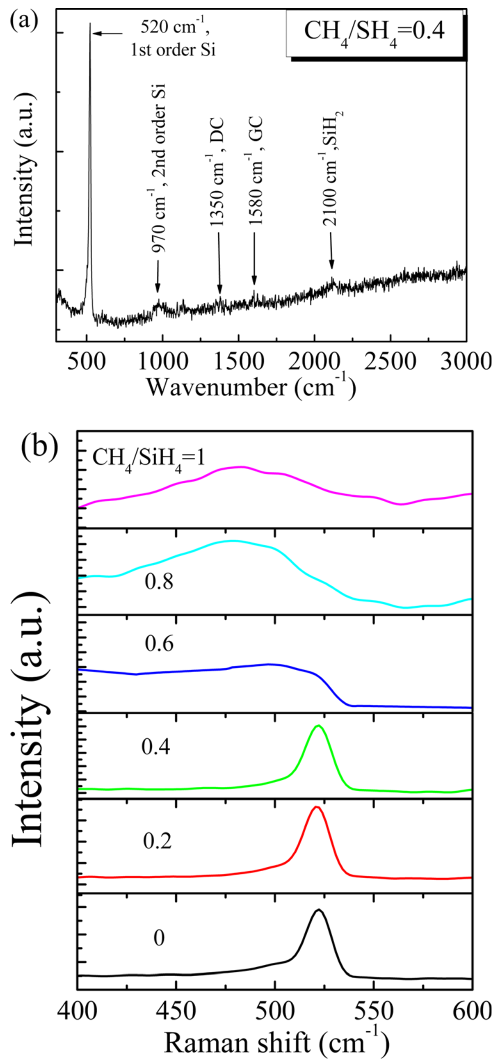

FIG. 5. The long wavenumber range Raman spectra (a) of the SiC thin film deposited at feedstock gas ratio $CH_4/SiH_4 = 0.4$, where the signals of Si–Si, C–C, and Si–H are observed, and narrow range Raman spectra of Si (b). Silicon changes from crystal ($\sim$521 cm^{-1}) to amorphous phase ($\sim$485 cm^{-1}) through an intermediate phase ($\sim$505 cm^{-1}).

ratios are presented in Fig. 5(b). One can find that the peak position is located at the vicinity of 521 cm^{-1} and remains unchanged when the gas ratio of CH_4/SH_4 is in the range of 0–0.4. This peak comprises three components: the TO mode of amorphous silicon peak at about 480 cm^{-1}, the intermediate phase around 510 cm^{-1} due to the occurrence of micro-grains of size no more than 30 Å,[25,26] and the crystalline silicon phase near 521 cm^{-1}. The crystalline fraction of Si in the thin films is estimated by the integrated areas ratio of crystalline phase plus intermediate phase to the total.[21] The calculated results show that the crystallinity of Si initially increases and then decreases slightly when the gas ratio CH_4/SH_4 is varied from 0 to 0.2 and then 0.4. Therefore, it is reasonably assumed that the incorporation of minority CH_4 molecules improves the silicon crystallinity and makes the silicon network more ordered. However, further increase of the CH_4 molecules deteriorates the silicon crystallinity. One can notice that, in Fig. 5(b), the peak of the Raman spectra is shifted to around 505 cm^{-1} at gas ratio of 0.6. As mentioned above, the occurrence of intermediate phase indicates the formation of nano-size silicon grains in the thin films. The nano level size of the silicon grains is calculated by the formula:[26] $t = 2\pi\sqrt{B/\Delta\omega}$, where t is the grain size, B ($\sim$2.0 cm^{-1} nm^2) is the FWHM of the Raman peak, and $\Delta\omega$ is the peak shift from nanocrystalline to crystalline silicon. The obtained value is $\sim$2.3 nm, which is out of the detection range of XRD. Considering the abrupt enhancement of PL in Fig. 4 at gas ratio $CH_4/SH_4 = 0.6$, we can reasonably attribute the distinct change of PL to the formation of a great deal of nano-size silicon grains. Actually, the crystal silicon quantum dots with dimension of 2–7 nm embedded in amorphous SiC matrix were directly observed using HRTEM method.[8] In combination with the size value from XRD, it can be concluded that addition of methane up to $CH_4/SH_4 = 0.6$ leads to the grains average size shrinkages from 26 nm to 2.3 nm. It is worthwhile to note that silicon becomes nearly amorphous with the peak at around 485 cm^{-1} when the ratio reaches 0.8 and above. The phase evolution of silicon and the PL process in our experiments should be related to the formation of amorphous SiC. While the information of the host matrix SiC where Si quantum dot is embedded in is yet deficient. For the purpose to characterize the Si–C bond, FTIR transmission spectra measurements were performed.

F. FTIR transmission spectra

Fig. 6 shows the FTIR transmission spectra of the thin films deposited at different gas ratios. The peak located at $\sim$635 and 2100 cm^{-1} corresponds to the Si–H rocking/wagging and the SiH_2 stretching modes, respectively.[27] With the increasing CH_4 in the feedstock gases, the former signal, which relates to the total hydrogen atoms bonded with silicon, starts to fade out. This fact implies that the incorporation of CH_4 results in the reduction of Si-bonded hydrogen in the deposited thin films. The mode at 790 cm^{-1}, assigned to Si–C stretching mode,[28] begins to emerge when $CH_4/SH_4 = 0.6$ and reaches its maximum at $CH_4/SH_4 = 1$. It is worthwhile to note that the intensity of this mode at $CH_4/SH_4 = 0.6$ is stronger than that at $CH_4/SH_4 = 0.8$, indicating more C atoms bonded with Si at $CH_4/SH_4 = 0.6$. Therefore, the sample at $CH_4/SH_4 = 0.6$ has a larger optical band gap than that at $CH_4/SH_4 = 0.8$ [Fig. 2(b)] even though the latter corresponds

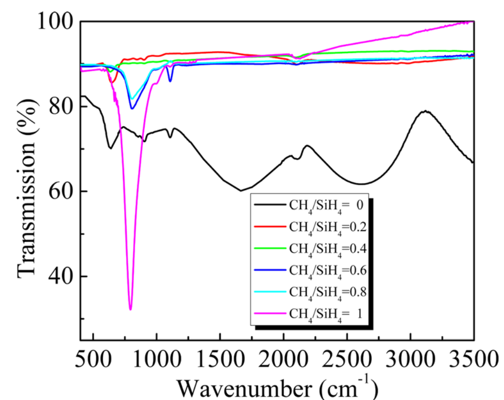

FIG. 6. FTIR transmission spectra of the thin films deposited at different gas ratios of CH_4/SiH_4. The Si–H wagging/rocking mode located around 635 cm^{-1} is weakened with increasing CH_4 content in the feedstock gases. On the contrary, the Si–C stretching mode is enhanced.

Downloaded 17 Jul 2013 to 155.69.4.4. This article is copyrighted as indicated in the abstract. Reuse of AIP content is subject to the terms at: http://jap.aip.org/about/rights_and_permissions

to more CH_4 flow rate. The shoulder at 1000 cm^{-1} and the small signal in the range of 2800–3100 cm^{-1} are assigned to the wagging/rocking and stretching modes of CH_n,[27] respectively. While the C–C bond corresponding signal located around 1600 cm^{-1} is absent, which, together with the result of Raman scattering, implies the limited number of C–C bond in the as-deposited thin films.

The mode located at ~1100 cm^{-1} due to Si–O stretching mode is clearly visible only at $CH_4/SH_4 = 0$ and 0.6. This seems to point to the comparatively higher oxygen content at these two points: $CH_4/SH_4 = 0$ where CH_4 is absent, and $CH_4/SH_4 = 0.6$ where the most intense PL occurs at around 880 nm. Because oxygen is usually involved in the PL process of Si based materials through the formation of defects level. In order to further understand the origin of present PL process, the XPS measurements were conducted.

G. XPS spectra

Fig. 7 displays the narrow-scan XPS spectra of Si *2 p* (a) and C *1 s* (b) in the synthesized thin films at different gas ratios of CH_4/SiH_4. At the four ratios of 0, 0.2, 0.4, and 0.8, the shapes of the Si *2 p* spectra are similar to each other with Si–Si/Si–H (99.3 eV) and Si–O_x (103.3 eV) and absence of Si–C (100.4 eV) signal.[29] In comparison, most of Si atoms bond with C in the absence of Si–O_x at the ratio of 0.6. When the ratio was increased from 0.6 to 0.8, the bond configurations of C, Si, and O encounter a distinct change. It is believed that this behavior should be originally related to the special interaction between SiH_4 and CH_4 accompanied with the etching effect of hydrogen in the inductively coupled high density plasma source. But the detailed mechanism is yet clear. At ratio of 1, all silicon atoms bond with C and Si–O_x signal disappears. In Fig. 7(b), three peaks located at around 283.2, 285, and 287.6 eV are ascribed to bonds of C–Si, C–C/C–H, and C–O, respectively.[29] In the ratio range of 0–0.4, most of the C atoms bond to C with a small number of C–O. At ratio 0.6 and 1, most of C atoms bond to Si with some minor C–C. At ratio of 0.8, C bonds to O, C, and Si. With exception of the bond configuration of O, the information in XPS is consistent with that in the FTIR spectra. This is attributed to the fact that XPS mainly detects the sample surface, which usually suffers from oxidation in air atmosphere.

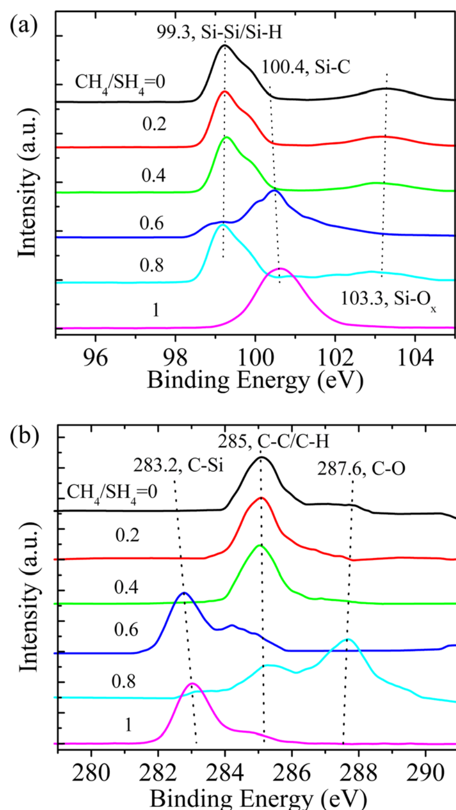

FIG. 7. The narrow scan XPS patterns of Si *2 p* (a) and C *1 s* (b).

IV. DISCUSSIONS

Most of the existing PL processes in silicon based materials are oxygen related, especially when the oxygen is intentionally introduced by thermal annealing. Furthermore, some oxygen-related defect models such as oxygen shallow donors (SDs) and nonbridging oxygen hole center (NBOHC) have been widely engaged.[30] The surface or subsurface is usually the source of PL process. From our experiment results, when the stronger PL is observed the oxygen content is very low. As a result, the possibility of main contribution from post-oxidation due to atmosphere exposure should be ruled out. Remarkably, the emission energy in PL spectra did not shift at all with the size reduction of the silicon grain even though the average size of <3 nm falls well into the region where quantum confinement effect applies. This is a strong evidence for excluding the main role of pure QSE model. In combination with our previous HRTEM observation, we can reasonably postulate the following scenario propose by Qin and Li[9] in nc-Si/SiO_2 system: Silicon QDs are embedded in host SiC matrix; photoexcited carries occur in Si QDs, while the radiative recombination of the photoexcited electron-hole pairs occurs in the luminescence centers (LCs) in the surrounding SiC or at Si/SiC interface. According to this model, PL intensity is mainly dependent on the density of LCs and QDs.

In present materials system, i.e., nc-Si/a-SiC, the LCs are originated from the incorporation of carbon atoms. Fig. 8 shows the carbon content calculated from the XPS measurement and the integrated PL intensity as a function of gas ratio CH_4/SiH_4. The carbon content and integrated PL intensity

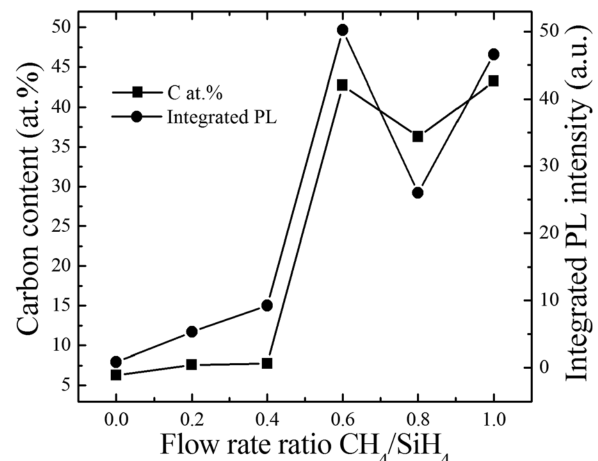

FIG. 8. The carbon content from XPS measurement and integrated PL intensity as functions of feedstock gas ratio of CH_4/SiH_4.

Downloaded 17 Jul 2013 to 155.69.4.4. This article is copyrighted as indicated in the abstract. Reuse of AIP content is subject to the terms at: http://jap.aip.org/about/rights_and_permissions

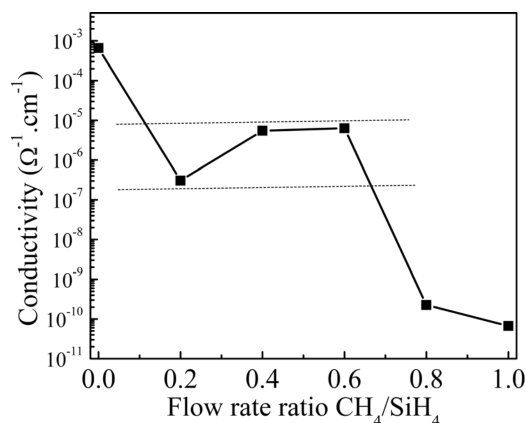

FIG. 9. The conductivity of the thin films deposited at different gas ratios of CH_4/SiH_4.

display the same trend with varying CH_4/SiH_4. Both of them increase gradually in the ratio range of 0–0.4, reach their maximum at ratio of 0.6, decline to a local minimum at ratio of 0.8, and then begin to increase again. The carbon content defines the density of LCs, where the light emission occurs through electron-hole pair's radiative recombination. Although carbon contents at ratio of 1 and 0.6 are comparable, the integrated PL of the former is still less than that of the latter. This is due to the larger nanocrystal QDs density at the ratio of 0.6, which is clearly evidenced by the Raman peak located at around 505 cm^{-1}.

Another evidence to support the nc-Si/a-SiC scenario is the conductivity of the thin films, which is shown in Fig. 9 at different gas ratios. The curve can be vertically separated into three regions: (i) without CH_4, (ii) intermediate CH_4 content ($CH_4/SiH_4 = 0.2$, 0.4, and 0.6), and (iii) high CH_4 content ($CH_4/SiH_4 = 0.8$ and 1). In region (i), the conductivity is comparatively high due to the low C content from the atmosphere contamination and high silicon crystallinity. From region (i) to (ii), the conductivity decreases drastically owing to the increase of carbon. It is worthwhile to note that the sample of $CH_4/SiH_4 = 0.6$ has conductivity competitive with that of $CH_4/SiH_4 = 0.4$ even though the former contains more wide band gap SiC (see Fig. 6). At ratio $CH_4/SiH_4 = 0.6$, high density nanocrystal Si QDs were formed and surrounded by SiC. The electronic transport is realized by the tunneling at the interface of Si and SiC, as described in the system of nanocrystal Si QDs/SiO_2.[31] In addition, SiC plays a passivation role on the dangling Si bands to facilitate the transport process. In region (iii), the conductivity is continuously decreased to the level of $10^{-11}\ \Omega^{-1}\ cm^{-1}$.

V. CONCLUSIONS

Amorphous SiC thin films were synthesized in the high density LFICP system using different compositions of CH_4 and SiH_4 diluted by H_2. With the gradual incorporation of CH_4 into the feedstock gases, silicon bond structure becomes more disordered and changes from crystalline to amorphous phase through an intermediate phase. At the intermediate ratio of $CH_4/SiH_4 = 0.6$, high density crystal Si QDs embedded in the SiC matrix were formed to construct a nc-Si/a-SiC system. The high density of Si QDs and SiC bonds facilitate the room temperature PL emission fixed at wavelength of around 880 nm. The photoexcitation occurs in the nc-Si QDs, whereas photoemission occurs in the amorphous SiC or at SiC-Si interface, as explained by the QCLC model.

ACKNOWLEDGMENTS

This work was supported by the National Research Foundation and the Agency for Science, Technology and Research for Singapore. Technical helps from Dr. J. W. Chai are highly appreciated. H. P. Zhou and D. Y. Wei acknowledge the research scholarship provided by the Nanyang Technological University.

[1]T. Chen, Y. Huang, H. Wang, D. Yang, A. Dasgupta, R. Carius, and F. Finger, Thin Solid Films **517**, 3513 (2009).
[2]T. Mueller, W. Duengen, Y. Ma, R. Job, M. Scherff, and W. R. Fahrner, J. Appl. Phys. **102**, 074505 (2007).
[3]I. Martín, M. Vetter, A. Orpella, J. Puigdollers, A. Cuevas, and R. Alcubilla, Appl. Phys. Lett. **79**, 2199 (2001).
[4]B. Racine, A. C. Ferrari, N. A. Morrison, I. Hutchings, W. I. Milne, and J. Robertson, J. Appl. Phys. **90**, 5002 (2001).
[5]C. Ehling, J. Werner, and M. Schubert, Phys. Status Solidi C **7**, 1016 (2010).
[6]M. Xu, S. Xu, J. W. Chai, J. D. Long, and Y. C. Ee, Appl. Phys. Lett. **89**, 251904 (2006).
[7]D. Y. Song, E. C. Cho, G. Conibeer, Y. Huang, C. Flynn, and M. Green, J. Appl. Phys. **103**, 083544 (2008).
[8]Q. J. Cheng, E. Tam, S. Xu, and K. Ostrikov, Nanoscale **2**, 594 (2010).
[9]G. G. Qin and Y. J. Li, Phys. Rev. B **68**, 085309 (2003).
[10]L. Houben, M. Luysberg, P. Hapke, R. Carius, F. Finger, and H. Wagner, Philos. Mag. A **77**, 1447 (1998).
[11]S. Mukhopadhyay, C. Das, and S. Ray, J. Phys. D: Appl. Phys. **37**, 1736 (2004).
[12]J. Tauc, *Amorphous and Liquid Semiconductor* (Plenum, New York, 1974), p. 159.
[13]Q. J. Cheng, S. Xu, and K. Ostrikov, J. Phys. Chem. C **113**, 14759 (2009).
[14]K. Bhattacharya and D. Das, Nanotechnology **18**, 415704 (2007).
[15]A. M. Ali, J. Lumin. **126**, 614 (2007), and references therein.
[16]Q. J. Cheng, S. Xu, J. D. Long, S. Y. Huang, and J. Guo, Nanotechnology **18**, 465601 (2007).
[17]G. Ledoux *et al.*, Phys. Rev. B **62**, 15942 (2000).
[18]M. Lannoo, C. Delerue, and G. Allan, J. Lumin. **70**, 170 (1996).
[19]A. G. Cullis and L. T. Canham, Nature (London) **353**, 335 (1991).
[20]F. Koch, V. Petrova-Koch, T. Muschik, A. Nikolov, and V. Gavrilenko, in Some Perspectives on the Luminescence Mechanism via Surface-confined States of Porous Si (Mater. Res. Soc. Symp. Proc., 1992), Vol. **283**, p. 197.
[21]H. P. Zhou, D. Y. Wei, S. Xu, S. Q. Xiao, L. X. Xu, S. Y. Huang, Y. N. Guo, W. S. Yan, and M. Xu, J. Appl. Phys. **110**, 023517 (2011).
[22]M. L. Brongersma, A. Polman, K. S. Min, E. Boer, T. Tambo, and H. A. Atwater, Appl. Phys. Lett. **72**, 2577 (1998).
[23]M. Park, C. W. Teng, V. Sakhrani, M. B. Mclaurin, R. M. Kolbas, R. C. Sanwald, R. J. Nemanich, J. J. Hren, and J. J. Cuomo, J. Appl. Phys. **89**, 1130 (2001).
[24]R. Hillel, M. Maline, F. Gourbilleau, G. Nouet, R. Carles, and A. Mlayah, Mater. Sci. Eng., A **168**, 183 (1993).
[25]H. S. Mavi, A. K. Shukla, S. C. Abbim, and K. P. Jain, J. Appl. Phys. **66**, 532 (1989).
[26]Y. He. C. Yin, G. Cheng, L. Wang, and X. Liu, J. Appl. Phys. **75**, 797 (1994).
[27]J. P. Conde, V. Chu, M. F. Silva, A. Kling, Z. Dai, J. C. Soares, S. Arekat, A. Fedorov, M. N. Santos, F. Giorgis, and C. F. Pirri, J. Appl. Phys. **85**, 3327 (1999), and references therein.
[28]J. Fonseca, S. Tasker, D. Apperley, and J. Badyal, Chem. Mater. **5**, 1676 (1993).
[29]J. Moulder, W. Stickle, P. Sobol, and K. Bomben, *Handbook of X-ray Photoelectron Spectroscopy* (Physical Electronics, Minnesota, 1995).
[30]A. G. Cullis, L. T. Canham, and P. D. J. Calcott, J. Appl. Phys. **82**, 909 (1997).
[31]G. G. Qin and Y. Q. Jia, Solid State Commun. **86**, 559 (1993).

Downloaded 17 Jul 2013 to 155.69.4.4. This article is copyrighted as indicated in the abstract. Reuse of AIP content is subject to the terms at: http://jap.aip.org/about/rights_and_permissions